Weakly Barred, Early-Type Ringed Galaxies. I. The Seyfert Galaxy NGC 3081

R. Buta – University of Alabama

Citation of published version:

Buta, R. (1990): Weakly Barred, Early-Type Ringed Galaxies. I. The Seyfert Galaxy NGC 3081. *The Astrophysical Journal,* 351(p. 62). DOI: http://dx.doi.org/10.1086/168444

THE ASTROPHYSICAL JOURNAL, 351:62–74, 1990 March 1

WEAKLY BARRED, EARLY-TYPE RINGED GALAXIES. I. THE SEYFERT GALAXY NGC 3081

R. BUTA
Department of Astronomy, University of Texas at Austin; and Department of Physics and Astronomy, University of Alabama
Received 1989 June 26; accepted 1989 August 25

ABSTRACT

Galaxies with bright rings, little gas, and little or no obvious bar are not adequately explained by current theories of ring formation in disk galaxies. This series focuses on four extreme examples which illustrate the diverging characteristics well. The galaxies are studied by means of multicolor CCD surface photometry obtained with the 3.9 m telescope of the Anglo-Australian Observatory.

The ringed Seyfert galaxy NGC 3081 is an S0/a system possessing an unusually high contrast inner ring enveloping a weak bar. In this first paper of the series, the structure of this galaxy is described using BVR_CI_C surface photometry. The observations reveal a complex system which shares many properties in common with NGC 1433, a prototype SB(r) type spiral with a strong bar. The bar of NGC 3081 is much weaker than that in NGC 1433, but the inner ring is more eccentric than those of most SB galaxies. Significant azimuthal variations in the color indices occur around the ring which are probably due to the elongated shape. It is suggested that while many properties of the three rings in this galaxy can be explained in terms of orbit resonance theory, the extreme shape of the inner ring and the weakness of the bar are contradictions to the theory that need to be addressed. It is suggested that NGC 3081 is a possible example of an object where secular dissolution of the bar is occurring.

Subject headings: galaxies: individual (NGC 3081) — galaxies: photometry — galaxies: Seyfert — galaxies: structure

I. INTRODUCTION

Early-type disk galaxies (stages $S0^+$ to Sa) provide some of the most spectacular examples of ring phenomena in the sky. It is among these galaxies where inner, outer, and nuclear rings appear most closed and well-defined, such that the term "ring" is entirely appropriate. In spirals having stage Sab or later, the same types of rings are observed but often they are pseudorings made up of part of the spiral pattern. In Sa, S0/a, and S0 galaxies, the spiral character of rings is less prominent, and it is among these galaxies where we can address a number of important problems of ring phenomena that may not be evident were we to focus on spirals alone.

The problems mainly concern ringed S0 galaxies. Two of the necessary ingredients for ring formation in spirals are thought to be the presence of a bar and of gas. If a bar is strong enough to induce orbit crossing near resonances, then dissipation in the gas flow can lead to spiral structure and naturally toward ring formation (Schwarz 1979). What is interesting is how there exist some S0 galaxies which provide a contradiction to this scenario: they have high contrast inner or outer rings and *little or no obvious bar*. When we consider the low gas content that S0 galaxies have compared to Sa or Sb spirals (Wardle and Knapp 1986), the problem is compounded. It is with these points in mind that I would like to examine carefully the properties of rings in apparently weakly barred or nonbarred early-type disk galaxies. I would like to know whether these rings share any characteristics in common with those in spirals, particularly those in classical barred spirals like NGC 1433 (Buta 1986*b*), or whether they might in some way be fundamentally different.

The galaxies to be discussed in this series are NGC 3081, NGC 7020, NGC 7187, and NGC 7702. Each is classified as type $S0^+$ in the system of the *Second Reference Catalogue of Bright Galaxies* (de Vaucouleurs, de Vaucouleurs, and Corwin 1976, hereafter RC2), and all were chosen from an extensive survey of southern ringed galaxies based on the SRC J Sky Survey charts (Buta 1986*a*). However, while these four objects are very good examples of ringed systems, each is near the extreme range in the strength of the ring enhancements and so cannot be regarded as typical.

In this first paper I present multicolor CCD surface photometry of NGC 3081, the only one of the four with a fairly obvious but weak bar. A well-known Seyfert 2 galaxy, NGC 3081 has been the subject of many papers concerned with its nuclear activity. Detailed studies of the nuclear emission-line shapes and intensities have been made by Véron (1981), Phillips, Charles, and Baldwin (1983), Whittle (1985), and Appenzeller and Ostreicher (1988). Martin *et al.* (1983) measured the polarization of the nucleus, and Wilson and Meurs (1982) measured the 1415 MHz continuum flux. Good photographs are presented in Sandage (1961), Kormendy (1979), and Simkin, Su, and Schwarz (1980). Narrow-band imaging and continuum flux distributions are presented by Durret and Bergeron (1986) and Boisson and Durret (1986). In the following analysis I shall focus mainly on the large-scale structure of NGC 3081 with little attention to the nucleus. The data are presented in the form of images, color index maps, brightness profiles, Fourier decompositions, and other information. Section II summarizes the observations made, while § III describes the morphology. The data analysis and discussion are presented in §§ IV and V, respectively. Conclusions are presented in § VI.

II. OBSERVATIONS

The observations were made with the prime focus RGO CCD camera on the 3.9 m Anglo-Australian Telescope in 1984 December. The camera used an RCA SID 53612 chip having 320 × 512 pixels, each 0".49 × 0".49 in size. Fringing was particularly severe in the R and I passbands (less so in the V band), but was mostly removable by a fringe map. The field used for

TABLE 1

OBSERVING LOG OF CCD IMAGES

Filter	Air Mass	Sky (ADU)	Exposure (s)	μ_s(Ap.) (mag s^{-2})	μ_s(S.S.) (mag s^{-2})	Seeing (FWHM)
B	1.023	275.0	500	22.55	22.54	2.″43
V	1.020	257.0	300	21.70	21.70	2.38
R	1.018	307.0	200	...	21.05	2.20
I	1.016	492.0	200	...	19.39	2.11

the fringe map came from a short list of candidate fields toward especially dark dust clouds in the Milky Way.

Table 1 gives an observing log of the images used for this paper. The images were taken with filters that match the Johnson *B* and *V* systems and the Cousins *R* and *I* systems. Reduction of the images followed standard procedures, and was performed using system routines at Mount Stromlo Observatory in the early phases of the work and later IDL on a University of Texas Microvax. For NGC 3081, the field of view (2.′6 × 4.′2) was only barely adequate for the sky subtraction. The sky subtraction will therefore provide one of the largest sources of uncertainty in the data presented here.

Calibration of the images was performed in two ways. First, several Landolt (1983) standard stars were observed to get the transformation coefficients of the CCD system. These stars did not have an adequate range in air mass to get reliable extinction coefficients, and it was necessary to use mean extinction coefficients for Siding Spring. The standard stars could be used to get zero points for all of the images, but I only used such zero points for the *R* and *I* passbands where no adequate photoelectric aperture photometry was available. For the *B* and *V* images, the zero point was obtained using aperture photometry alone, taking into account transformation coefficients derived from the standard stars. The photoelectric photometry was taken from Longo and de Vaucouleurs (1983, 1985). Table 1 lists the zero points as μ_s, the surface brightness of the night sky. For *B* and *V*, the values from aperture photometry μ_s(Ap.) and from standard stars μ_s(S.S.) are given. These show good agreement, which gives me confidence that the night was photometric and that the zero points in *R* and *I* are reliable. Estimates of the seeing for each image are also given in Table 1.

III. MORPHOLOGY

Figures 1 and 2 (Plates 1–2) show the *B* and *I* band images of NGC 3081, respectively. The images are displayed in real surface brightness units (i.e., mag s^{-2}, fully calibrated for zero point) to show the interesting structure which is present over a wide range of surface brightness. The most striking characteristics of the galaxy are the inner ring and oval bulge, which are the only features visible in the photograph of this galaxy in the Hubble Atlas (Sandage 1961). On the deeper CCD images, a weak bar is also visible, and the disk of the galaxy is prominent as a very faint outer ring. This latter feature is shown better in photographs given by Kormendy (1979) and Simkin, Su, and Schwarz (1980).

Additional interesting features of the galaxy are the dust lanes visible in the weak bar. These are difficult to see in the direct images, but they are plainly visible in the $B-I$ color index map illustrated in Figure 3 (Plate 3). This map is coded such that "blue" features are dark while "red" features are light. It shows that the dust lanes appear to curve toward the elongated core in a manner very reminiscent of what is observed in the SB(r) spiral NGC 1433 (Buta 1986*b*). The dust lanes are, however, much more subtle than in NGC 1433 and more curved.

The $B-I$ color index map also shows the very interesting manner in which recent star formation is distributed in this galaxy: the inner ring is a closed and well-defined blue enhancement that is slightly pointed at the major axis. It looks more enhanced (bluer) in arcs along its major axis (this is quantified later) than along its minor axis and has a feathery or patchy character. In the center the nuclear oval shows an enhanced blue rim and is thus really a nuclear ring. The major axis of the nuclear ring oval does not align with that of the inner ring. The region between the two rings including the bar is almost of uniform color except for the weak dust lanes. For comparison, in NGC 1433 a nonaxisymmetric color gradient was found in this kind of region (Buta 1986*b*). Beyond the inner ring only a slight contrast of color is evident. The short spiral arcs lying just outside the inner ring major axis are clearly visible, however, and are apparently also sites of some recent star formation.

The CCD images suggest that NGC 3081 is not a late S0 but a very early type spiral. The blue-light image shows that at least three, and perhaps four, weak spiral arms emerge from near the major and minor axis points of the inner ring and that two weak spiral arcs form a small part of the outer ring. Also, Sandage (1961) has pointed out that the inner ring itself appears to be made of two tightly wound spiral arms. These characteristics suggest that the RC2 classification of the galaxy should be slightly revised, and I propose using (R)SAB(r, nr) 0/a, where (nr) is meant to recognize the nuclear ring (see Buta 1989). This revised type does not weaken the usefulness of NGC 3081 as a member of the present sample, but it does show that in many respects the galaxy is simply an earlier type version of NGC 1433 [type (R′)SB(r, nl)ab] with a weaker bar. More quantitative comparisons are made in the next sections.

IV. DATA ANALYSIS

a) Integrated Properties

The surface photometry was used first to measure the integrated magnitude and colors, concentration indices, effective parameters, and the quartiles of the light distribution of NGC 3081. Table 2 summarizes these parameters. The total magnitude B_T was obtained by integrating the light in elliptical annuli having the shape of the outer disk. For NGC 3081, I could not use an outer isophote ellipse fit to get this shape because the galaxy was too large compared to the width (2.′6) of the field. Instead, I have approximated this shape using the shape of the ridge line of the outer ring. Once the disk shape was adopted, an elliptically averaged luminosity profile within this shape was calculated, and for B_T, was extrapolated to infinity by assuming an exponential distribution in the outer

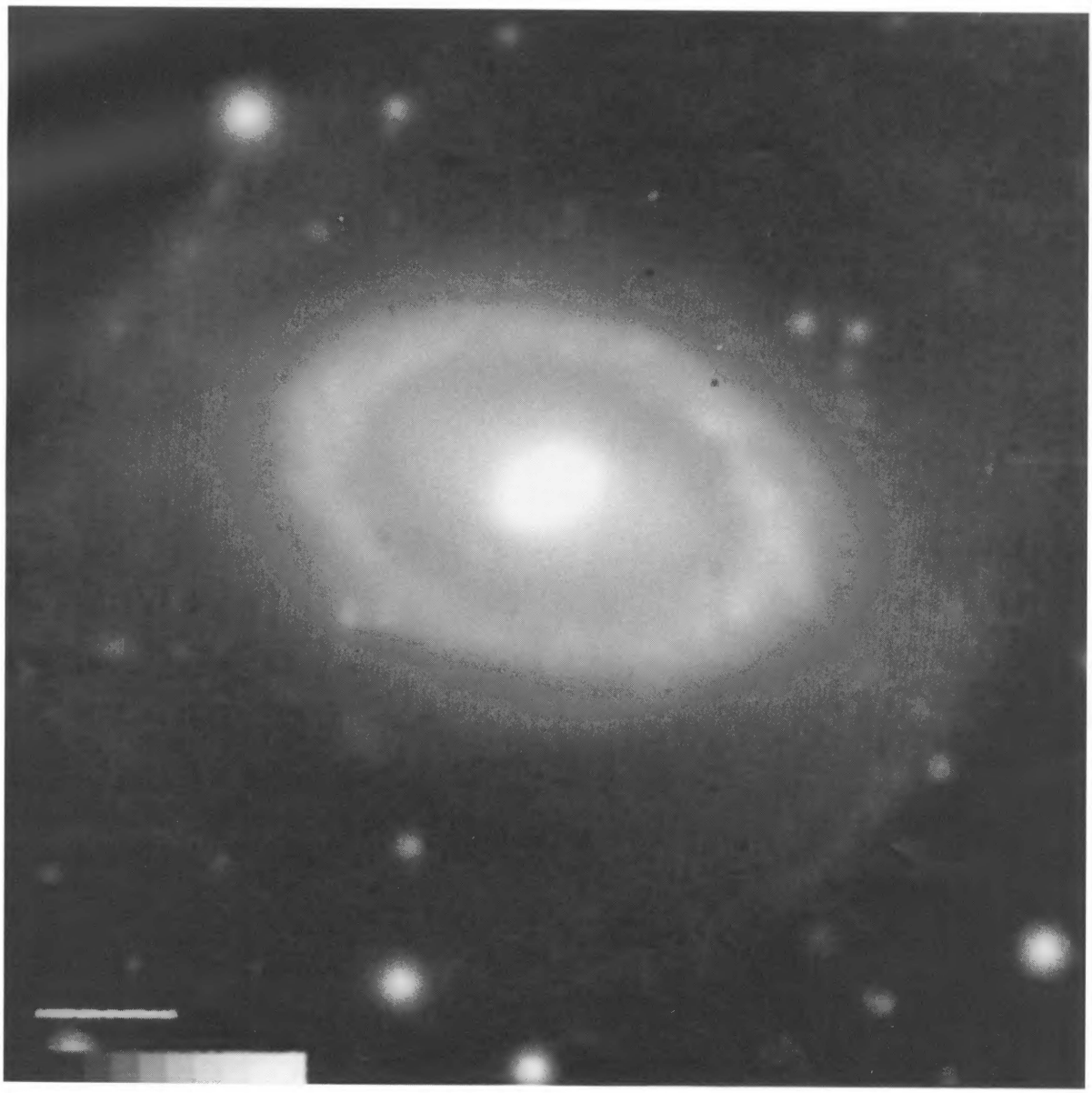

FIG. 1.—*B* band CCD image of NGC 3081 (500 s exposure). This and the two successive images have north at the top and east to the left. The white bar is 20″ in length. The step scale ranges from 18.0 to 28.0 mag s^{-2} in 0.5 mag s^{-2} steps.

PLATE 2

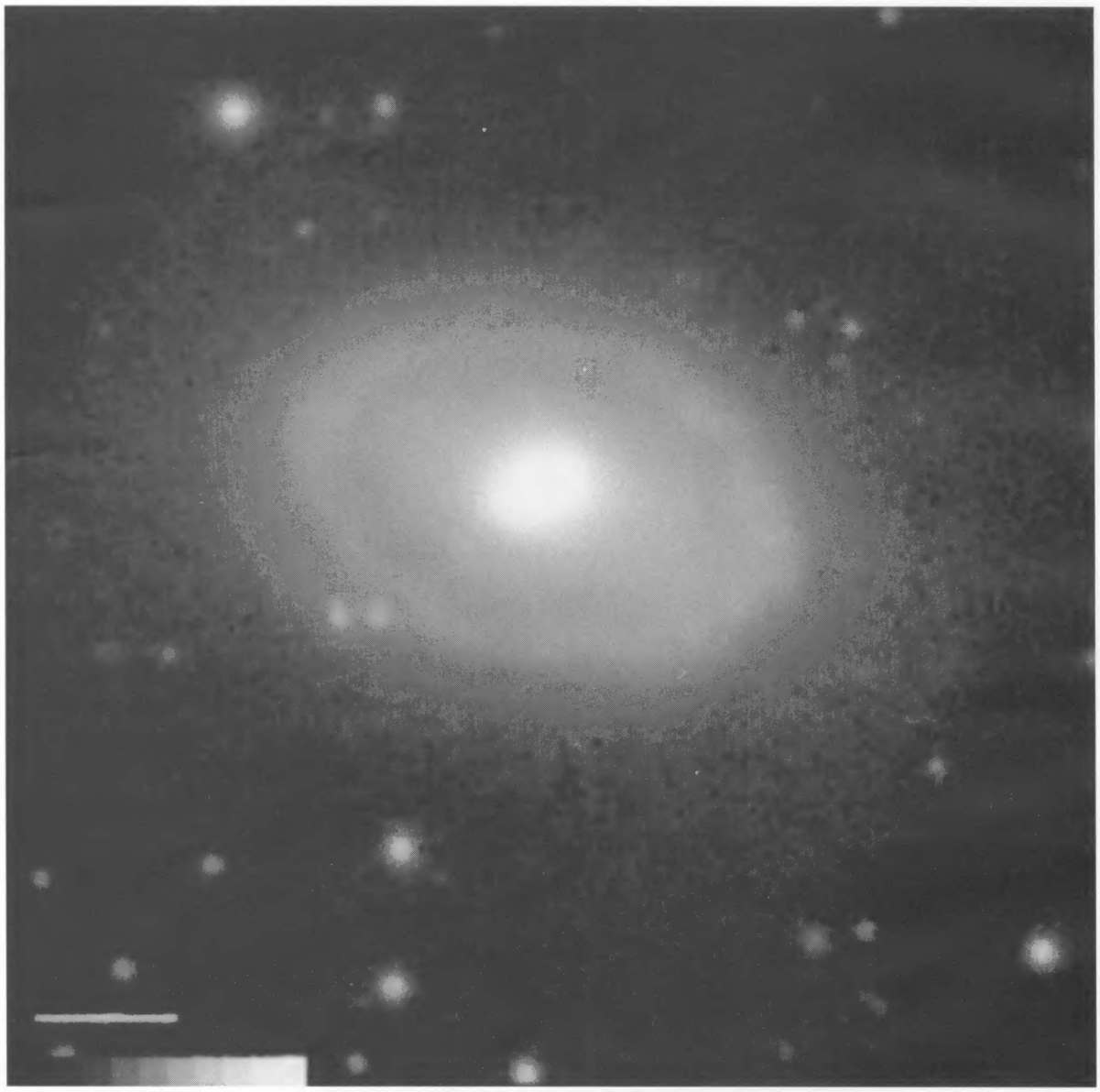

FIG. 2.—*I* band CCD image of NGC 3081 (200 s exposure). The white bar is 20″ in length. The step scale ranges from 16.0 to 26.0 mag s^{-2} in 0.5 mag s^{-2} steps.

BUTA (*see* **351**, 63)

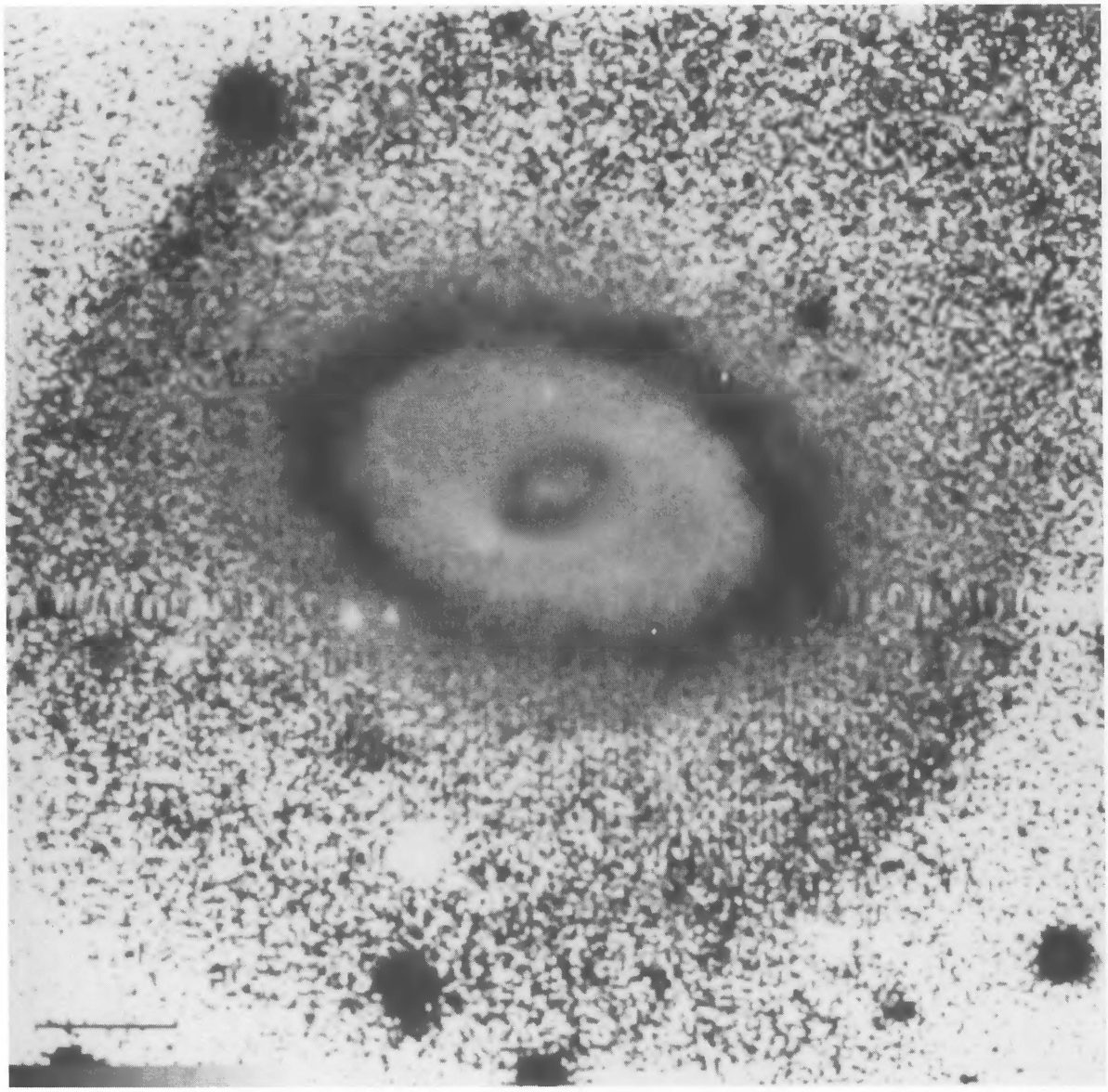

FIG. 3.—$B-I$ color index map of NGC 3081. The dark horizontal bar is 20″ in length. The step scale ranges from $B-I = 1.7$ (darkest) to 2.7 (lightest) in 0.1 mag steps.

TABLE 2

BASIC AND INTEGRATED PARAMETERS

Parameter	Value
α(1950)	$09^h57^m10^s.0$
δ(1950)	$-22°35'09''.5$
l	259°.02
b	+25°.04
SGL	133°.2
SGB	−46°.1
RC2 type	(R)SAB(r)0$^+$
RSA type[a]	SB(s)a
Adopted type	(R)SAB(r, nr)0/a
B_T	12.85 ± 0.05
log A_e	0.93
m'_e	12.99 mag m^{-2}
$(B-V)_T$	0.88
$(U-B)_T$	0.34
$(V-R)_T$	0.60
$(V-I)_T$	1.32
log D_{25}	1.35
log R_{25}	0.22
θ_{25}	68°
$C_{21}(B)$	2.68
$C_{32}(B)$	1.74
r_1^*	0'.147
r_e^*	0'.394
r_3^*	0'.686
μ_1	21.63 mag s^{-2}
μ_e	22.57 mag s^{-2}
μ_3	24.34 mag s^{-2}
i	33° ± 5°
$(B-V)e$	0.93
$(U-B)e$	0.35
$(V-R)e$	0.60
$(V-I)e$	1.31

[a] Sandage and Tammann 1981.

parts. The amount of extrapolation required was only 0.09 mag from the last point on the profile.

The distance to NGC 3081 is estimated from its redshift since the inclination is too low for the Tully-Fisher relation to be useful. The mean redshift from five sources in the *Third Reference Catalogue of Bright Galaxies* (de Vaucouleurs *et al.* 1989, hereafter RC3), is 2383 km s^{-1}. To get the distance, I first correct the velocity to a frame of reference where the Hubble constant is largely independent of direction (de Vaucouleurs and Peters 1981; de Vaucouleurs *et al.* 1981; Buta and de Vaucouleurs 1983*b*). The corrected radial velocity of NGC 3081 is 2253 km s^{-1}, so using $H_0 = 100$ km s^{-1} Mpc^{-1}, then the distance is 22.5 Mpc. Using RC2 procedures to correct the total magnitude, then the absolute magnitude of NGC 3081 is $M_T^c(B) = -19.5$.

Since the integrated color/magnitude profiles reflect the quality of the calibrations, these are illustrated in Figure 4. The agreement between the observed magnitude/aperture and color/aperture relations with the simulated ones is good for V and $B-V$. Also shown in Figure 4 is the $U-B$ color versus aperture relation, which highlights an inverse integrated color-gradient characteristic more of a late-type spiral rather than an early-type one (see Fig. 6 of RC2). This is caused by the significant amount of star formation in the center of the galaxy. The corrected colors, $(B-V)_T^c = 0.73$ and $(U-B)_T^c = 0.25$ (both following RC2 procedures), are bluer than the average S0/a galaxy (de Vaucouleurs 1977).

Parameters at the quartiles of the B light distribution (concentration indices C_{21} and C_{32}, equivalent radii r_1^*, r_e^*, and r_3^*, and corresponding surface brightnesses μ_1, μ_e, and μ_3) were

TABLE 3

RING DIAMETERS, AXIS RATIOS, AND ORIENTATIONS

Parameter	Value
d(nr)	0'.22
q(nr)	0.69
θ(nr)(1950)	115°
d(r)	1'.11
q(r)	0.66
θ(r)(1950)	71°
d(R)	2'.46
q(R)	0.84
θ(R)(1950)	123°

obtained from an equivalent luminosity profile and integration table (de Vaucouleurs 1948, 1953) and provide useful data for quantitative morphology. The concentration indices are consistent with a strongly concentrated system, but probably are lower than might be expected because of the significant amount of light contained in the extended, bright inner ring. The amount of light inside the inner ring can be estimated from the integration table. Defining the inner ring/lens/bar region to be from $\mu_B = 21.5$ to 23.0 mag s^{-2}, I find that it contains about 40% of the total B band luminosity.

b) *Ring Shapes and Orientations*

Table 3 gives estimates of the apparent shapes and orientation of the three rings in this galaxy. The rings were defined interactively using a TV display and placing a cursor to mark positions along the ridge lines. This was done more than once for each ring at different times to check for internal consistency, and in all cases the independent estimates agreed very well in the derived apparent shape parameters. These parameters were derived by fitting an ellipse to the ridge line points.

The intrinsic shapes and orientations of the rings with respect to the bar are of great importance but are difficult to obtain accurately from the CCD images owing to the limited field of view. As mentioned in the previous section, it was necessary to define the orientation parameters of the system using the apparent shape of the faint outer ring. This gives a major axis position angle $\theta(R) = 123° \pm 4°$ and an axis ratio $q(R) = 0.84 \pm 0.04$. The position angle is referred to a 1950 coordinate system defined by reference to local SAO catalog stars. If the outer ring is intrinsically circular, then the implied inclination is $i \approx 33° \pm 5°$. The low inclination is consistent with the small velocity gradients ($\Delta V < 100$ km s^{-1}) measured by Durret and Bergeron (1986) from slit spectra. However, if the outer ring of NGC 3081 is an intrinsically oval feature embedded within a more axisymmetric disk, which is sometimes seen in galaxies of its type, then the adopted orientation parameters could be wrong by a large amount.

Of significance is how the shape and orientation parameters of the outer ring differ from the same parameters for the inner ring: $\theta(r) = 71° \pm 1°$ and $q(r) = 0.66 \pm 0.01$. The relative angle between the inner and outer rings, 52° ± 4°, agrees well with a completely independent earlier visual estimate, 56°, made from an SRC J Southern Sky Survey film and is also confirmed by the deep photograph given by Kormendy (1979). The inner and outer rings therefore must have rather different intrinsic shapes. We cannot reliably assess the intrinsic shape of the outer ring, except to note that statistics of apparent SB outer ring shapes (Buta 1984, 1986*a*; Schwarz 1984*a*) suggest that

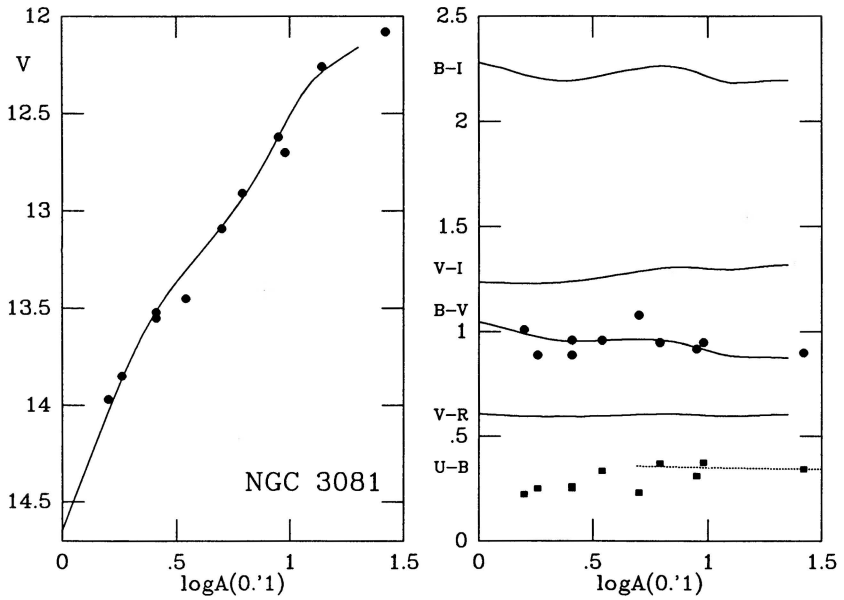

FIG. 4.—Magnitude vs. aperture and color vs. aperture relations for NGC 3081. The solid curves are simulations from the CCD surface photometry, and the data points are measured photoelectric values. The dashed curve for $U-B$ is based on an RC2 standard color curve and was used to extrapolate the integrated color, $(U-B)_T$.

they are mildy oval on average, with true axis ratios $q_0(\mathrm{R}) = 0.85$–0.90, and that most are aligned perpendicular to the bar. If we assume that the outer ring of NGC 3081 is intrinsically circular, which is not ruled out by statistics, then the intrinsic axis ratio of the inner ring would be about 0.61. If, as could be more likely, the outer ring is intrinsically oval with an axis ratio of 0.85 and aligned perpendicular to the bar, then the intrinsic axis ratio of the inner ring would be closer to 0.75. Both estimates are comparable to that found for the inner ring of NGC 1433: $q_0(\mathrm{r}) = 0.65 \pm 0.03$. Statistics favor an average axis ratio for SB inner rings of about 0.8 (Buta 1984, 1986*a*; Schwarz 1984*a*), so both NGC 1433 and NGC 3081 have inner rings more elongated than the mean.

For the nuclear ring, the projected parameters were derived from an ellipse fitted to the ridge line of the color enhancement, since the ring itself is not well differentiated in blue light. The apparent major axis position angle of this structure is displaced less than 10° from that of the outer ring, and the projected axis ratio of 0.69 leads to a deprojected axis ratio of about 0.82. Hence, the nuclear ring of NGC 3081 may be intrinsically more circular than the inner ring, an observation which is consistent with statistical studies (Buta 1984, 1986*a*). Its axis of elongation is also displaced from the bar/inner ring axis by about 49°, in a manner very similar to that of the nuclear ring/lens of NGC 1433.

The position angle of the bar was estimated using an ellipse fitted to the isophote having $\mu_I = 20.5$ mag s^{-2} (see next section). The angle is $\theta(\mathrm{B}) = 66° \pm 2°$, giving the apparent relative angle between the bar and inner ring as $|\theta(\mathrm{Br})| = 5° \pm 2°$ in projection. The true angle is obtained approximately by deprojecting the inner ring and bar axes; for the inner ring the position angle of the deprojected major axis is $\theta_0(\mathrm{r}) = 60°$, while that for the bar is $\theta_0(\mathrm{B}) = 62°$. Thus, $|\theta_0(\mathrm{Br})| = 2° \pm 3°$, implying that within the uncertainties the inner ring is intrinsically elongated along the axis of the weak bar. This alignment is important for understanding the nature of the inner ring and is consistent with the results of statistics of SB inner ring orientations (de Vaucouleurs and de Vaucouleurs 1964; Kormendy 1982; Buta 1984, 1986*a*; Schwarz 1984*a*). Since the galaxy is nearly face-on, this fact does not depend significantly on the choice of orientation parameters.

c) Ring Diameters

Table 3 also gives the apparent major axis diameters of the three rings of NGC 3081. Using a distance of 22.5 Mpc from the redshift, the linear diameters in projection are 1.5, 7.3, and 16.1 kpc for the nuclear, inner, and outer rings, respectively. For comparison, the systematics of ring sizes were extensively studied by de Vaucouleurs and Buta (1980*a*, *b*), Buta and de Vaucouleurs (1982, 1983*a*), and Buta (1984). The biggest inner rings were shown by Buta and de Vaucouleurs (1982) to occur in luminosity class I barred (SB) spirals at stage Sab along the revised Hubble sequence. For earlier type galaxies only the type dependence could be evaluated, and for stage S0/a Buta and de Vaucouleurs (1982) estimated $\langle \log D_r \rangle = 3.69 \pm 0.17$ (s.d.), or $D_r = 4.8\ (+2.4, -1.5)$ kpc. Since Buta and de Vaucouleurs did not allow for the intrinsic elongated shapes of inner rings in their analysis, it is best to compare these values with the diameter of NGC 3081's inner ring as seen in projection. The size appears to be near the upper limit of SAB inner rings and is more typical of the size in an SB(r)0/a galaxy [$D_r = 6.9$ $(+3.3, -2.2)$ kpc].

Nuclear rings are observed from stages S0$^+$ to Sc, and their diameters appear to have a small dependence on type (Buta 1984). Near stage S0/a the average size of such rings in SAB and SB galaxies is $D(\mathrm{nr}) = 1.7$ $(+1.3, -0.8)$ kpc (s.d.). The typical size of outer rings in SA, SAB, and SB galaxies is 14.5 $(+6.9, -4.7)$ kpc (s.d.). Thus the rings of NGC 3081 have sizes which are consistent with the means derived from other galaxies.

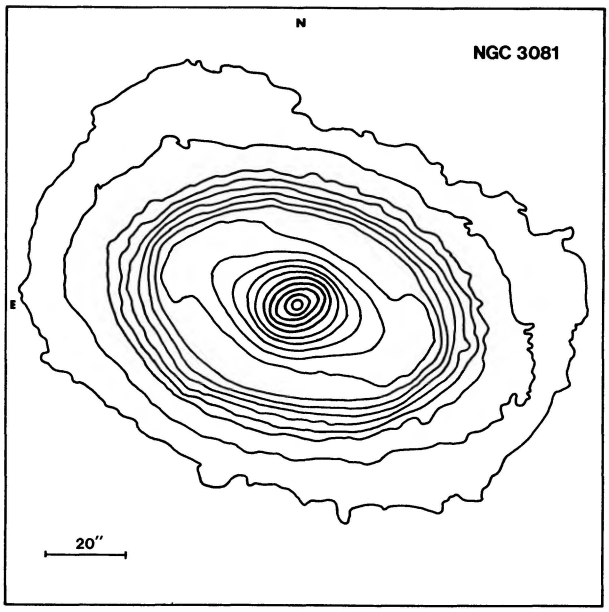

FIG. 5.—*I* band isophotes of the large-scale structure of NGC 3081. Different levels of smoothing were used for the plot, depending on surface brightness. The two largest isophotes correspond to $\mu_I = 22.5$ and 23.0 mag s^{-2} and were smoothed using a 5.″9 × 5.″9 box average. The next 11 isophotes range from $\mu_I = 22.0$ to 19.5 mag s^{-2} in steps of −0.25 mag s^{-2}, while the remaining five range from $\mu_I = 19.0$ to 17.0 mag s^{-2} in steps of −0.5 mag s^{-2}. All these were smoothed using a 3″ × 3″ box average.

d) Isophotes and Luminosity Profiles

A low-resolution isophote map of NGC 3081 is shown for the *I* band in Figure 5. The weak bar of the galaxy is displayed prominently in this figure. A high-resolution map in Figure 6 shows that a nuclear bar lies in the center. In projection this small bar is misaligned with the primary bar by 50° and lies

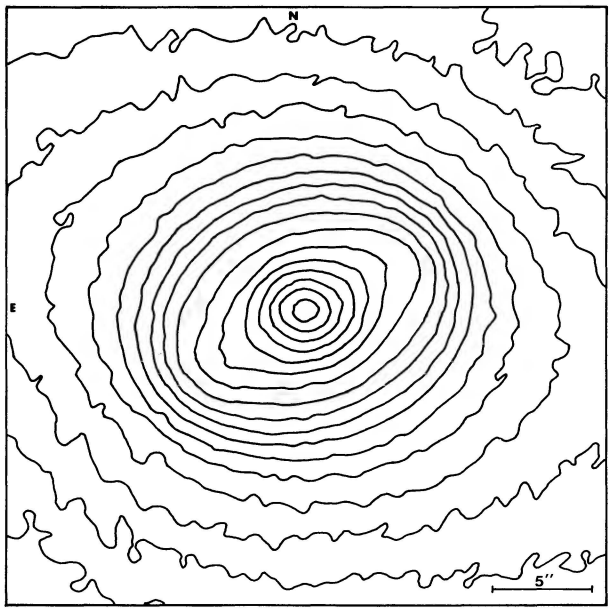

FIG. 6.—*I* band isophotes of the center of NGC 3081, showing the nuclear bar. The brightest isophote is at $\mu_I = 16.5$ mag s^{-2}, and each successive isophote is separated by 0.25 mag s^{-2}.

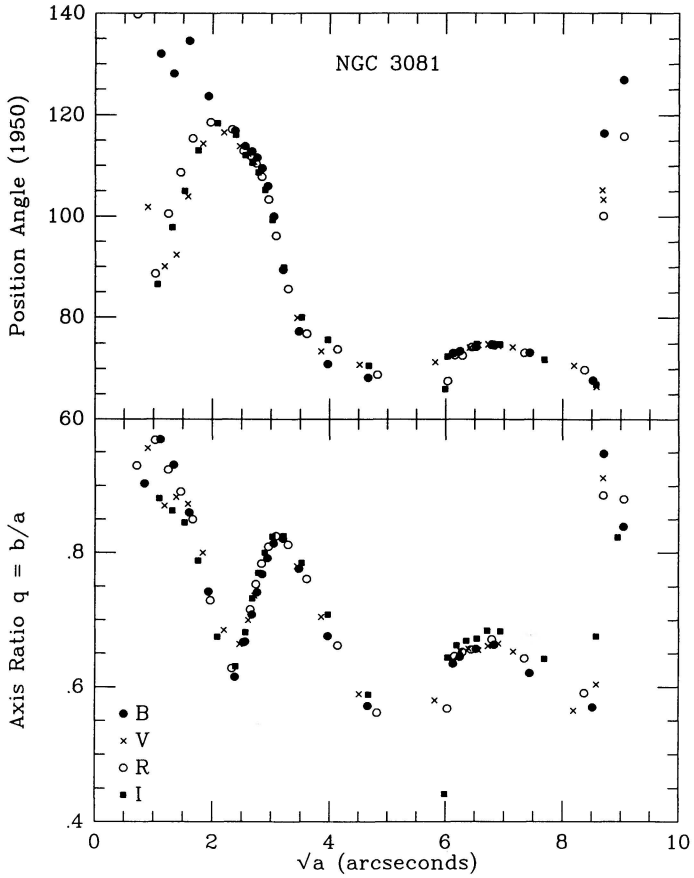

FIG. 7.—Dependence of isophote shapes and orientations on position within NGC 3081, based on ellipse fits.

nearly along the major axis of the nuclear ring. The feature has a diameter of 10.″5 (1.1 kpc) at the surface brightness level of $\mu_I = 18.0$ mag s^{-2}, and is also visible in the isophote images shown by Durret and Bergeron (1986). The presence of a nuclear bar is another property which makes this galaxy similar to NGC 1433.

The shapes and orientations of the isophotes as a function of radius are shown in Figure 7. All the available passbands were used for this plot. These plots bear a strong resemblance to those obtained for NGC 1433 (Fig. 5 of Buta 1986*b*). In the very center the isophotes are nearly round, but the axis ratio, *q*, drops to about 0.6 at the position of the nuclear bar. Then *q* rises to about 0.8 in the zone between the nuclear ring and the primary bar. In NGC 1433, isophotes become perfectly circular in this transition zone. A large change in position angle occurs across this zone in NGC 3081, just as in NGC 1433, and a roughly uniform position angle is found in the bar/inner ring region. The next significant change in axis ratio and orientation of the isophotes occurs in the outer parts of the faint outer ring, again very similar to what was found for NGC 1433.

The isophotes also show striking departures from elliptical shapes in some regions. Between the inner and outer rings, the isophotes of NGC 3081 in all passbands look distinctly boxy, and it is interesting that the same effect was observed in the same kind of region in NGC 1433 (see Fig. 6*d* of Buta 1986*b*). A useful way of quantifying these departures from elliptical shapes is to make a Fourier analysis of the deviations of

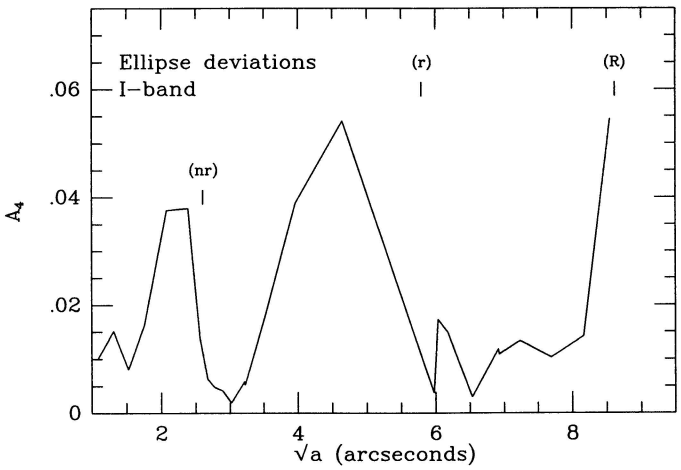

FIG. 8.—Relative amplitude of the 4θ Fourier component for I band isophotes. The major axis positions of the nuclear ring, inner ring, and outer ring are indicated.

an isophote from its fitted ellipse, a procedure which has recently been frequently applied to elliptical galaxies. Here I have used the technique as described by Bender and Möllenhoff (1987), and only the I band image was used to avoid too much influence by recent star formation on the isophote shapes. The fitted ellipse to an isophote was used to deproject that isophote, and the deviations from the radius were expanded in Fourier series. Denoting the sin 4θ amplitude as a_4 and the cos 4θ amplitude as b_4, then the relative total amplitude was derived as $A_4 = (a_4^2 + b_4^2)^{1/2}/a$, where a is the semimajor axis of the fitted ellipse. Figure 8 shows how A_4 varies with radius $(a)^{1/2}$. The amplitude could only be derived reliably to $a = 74''$, because isophotes larger than this became too noisy. The results show three regions having significant 4θ amplitude, one at $a = 5''$ associated with the nuclear bar (which is a pointed oval), one at $a = 22''$ associated with the primary bar, and one near and probably also somewhat beyond $a = 73''$ associated with the region between the inner and outer rings. These boxy or pointy zones are plainly visible in the isophote maps and the deviation from ellipses are large, about 4%–5% of the radii.

The complex structure of this galaxy is further reflected in luminosity profiles. One pair of profiles (Fig. 9) follows the major and minor axes of the inner ring, while the other set (Fig. 10) follows the major and minor axes of the outer ring. Color index profiles along each axis are also shown in these figures. Each ring produces a hump in the luminosity profiles, or a dip in the color profiles, wherever crossed, and the nuclear and outer rings are most prominent along the major axis of the outer ring while the inner ring is most prominent along its major axis. The inner ring achieves a surface brightness at its peak (along its major axis) of $\mu_B = 22.1$ mag s^{-2} at $r = 32''$, but the bluest colors are achieved at $r = 38''$. The peak surface brightness along the minor axis of the inner ring at $r = 21''.5$ occurs at $\mu_B = 22.5$ mag s^{-2}. The nuclear ring hump at $r = 5''$ along p.a. = 123° occurs at $\mu_B = 19.9$ mag s^{-2}, while the outer ring hump at $r \approx 74''$ along the same p.a. occurs at $\mu_B = 25.6$ mag s^{-2}. Since no part of any of the four sets of profiles shown can be regarded as $r^{1/4}$ bulge-dominated or exponential disk–dominated, the usual techniques of decomposition are not applicable to this galaxy and could be misleading if applied.

The color profiles in Figures 9 and 10 show just how extensive the star-forming zones of the rings really are. Along its

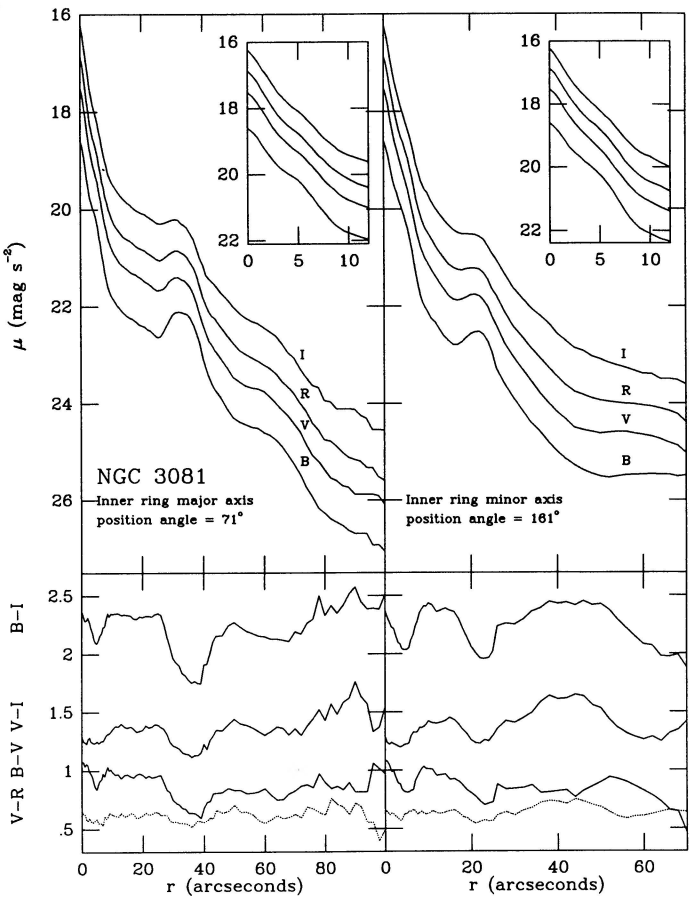

FIG. 9.—Surface brightness profiles along the major and minor axes of the inner ring of NGC 3081.

major axis, the inner ring has a full width of about $24'' = 2.5$ kpc. In fact, the width of the star-forming zone varies around the ring. This is illustrated in Figure 11 which shows isochromes of the inner ring for colors between $B-I = 1.8$ and 2.3. Most interesting is that for $B-I = 2.00$, which is about halfway between the color at the ring peak and the region just inside the ring. Denoting the semimajor axis radius of the ring peak by a_r, this plot illustrates how the shapes of the isochromes are more elongated for $a > a_r$ than for $a < a_r$. The results of ellipse fits to five isochromes (inner and outer $B-I = 2.00$, inner and outer $B-I = 2.10$, and inner $B-I = 2.20$) are given in Table 4. For the best defined isochromes at 2.0 and 2.1, the axis ratio decreases from about 0.69

TABLE 4

SHAPES OF ISOCHROMES

Feature	$B-I$	a	q	Position Angle
(nr)	2.10	8".1	0.67	116°.5
	2.15	8.6	0.71	114.2
	2.20	9.2	0.74	108.1
(r)	2.00	28.7	0.70	71.0
	2.00	41.8	0.59	72.0
	2.10	27.5	0.67	72.3
	2.10	45.3	0.59	73.4
	2.20	26.1	0.65	75.8

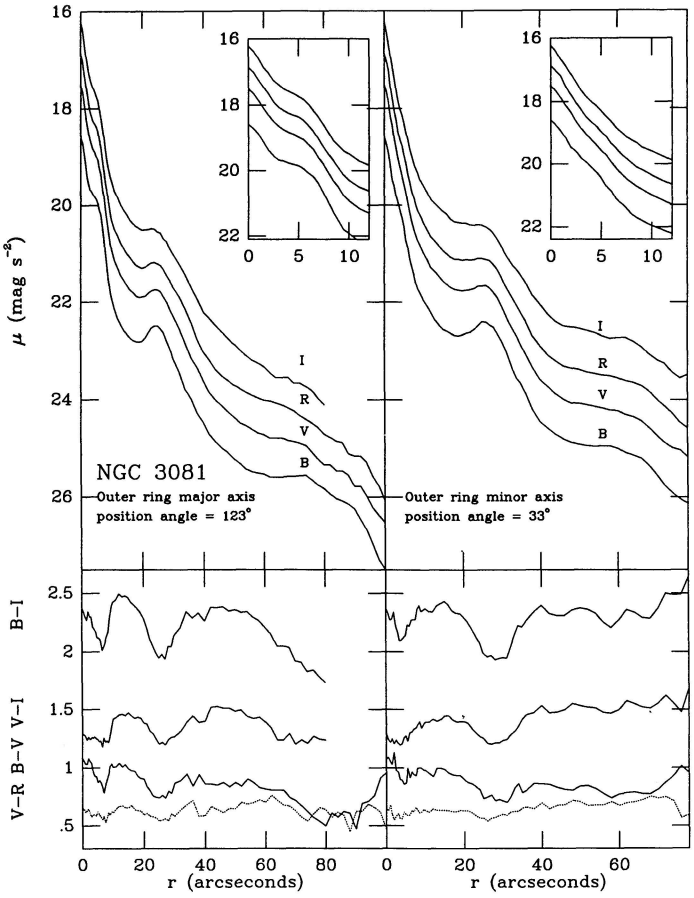

FIG. 10.—Surface brightness profiles along the major and minor axes of the outer ring of NGC 3081.

to 0.59 over the zone from $a = 28''$ to $a = 43''$. Across this same range, which corresponds to 1.6 kpc in projection, the position angle decreases by only about 1°. Thus, the inner ring is broader at its major axis than its minor axis by more than a factor of 2 between these isochromes.

Of equally interesting behavior are the isochomes of the nuclear ring. Only three could be fitted over a small range; these are compiled in Table 4 also. The fits show that the isochromes of the nuclear ring become less elongated with increasing a. The bluest isochrome ($B-I = 2.10$) is the most elongated.

e) *Elliptically Averaged Profiles and Fourier Intensity Amplitudes*

The nonaxisymmetric component in NGC 3081 was studied by means of a Fourier analysis of the *intensity distribution* (as opposed to the residuals of an ellipse fit about a single isophote). The analysis is made by deprojecting the galaxy and expanding the intensity distribution in Fourier series (see Buta 1986*a*). In principle the sums go from $m = 0$ to infinity, but in practice only the $m = 0$–6 terms are needed. The $m = 0$ term corresponds to an elliptically averaged profile and is compiled for each passband in Table 5 and illustrated for each in Figure 12. Deprojection of the galaxy was performed using the outer ring axis ratio and position angle in Table 3, so I am assuming that this feature is intrinsically circular. The elliptically averaged profiles for NGC 3081 bear much resemblance to those for NGC 1433. For both galaxies, the inner ring is spread over a broad range in this kind of profile because of its significant intrinsic elongation.

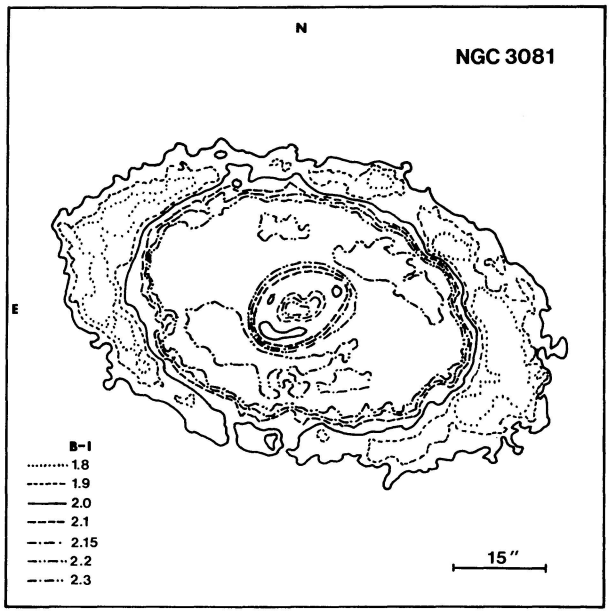

FIG. 11.—Isochromes of the inner regions of NGC 3081. The legend at lower left shows the contours illustrated.

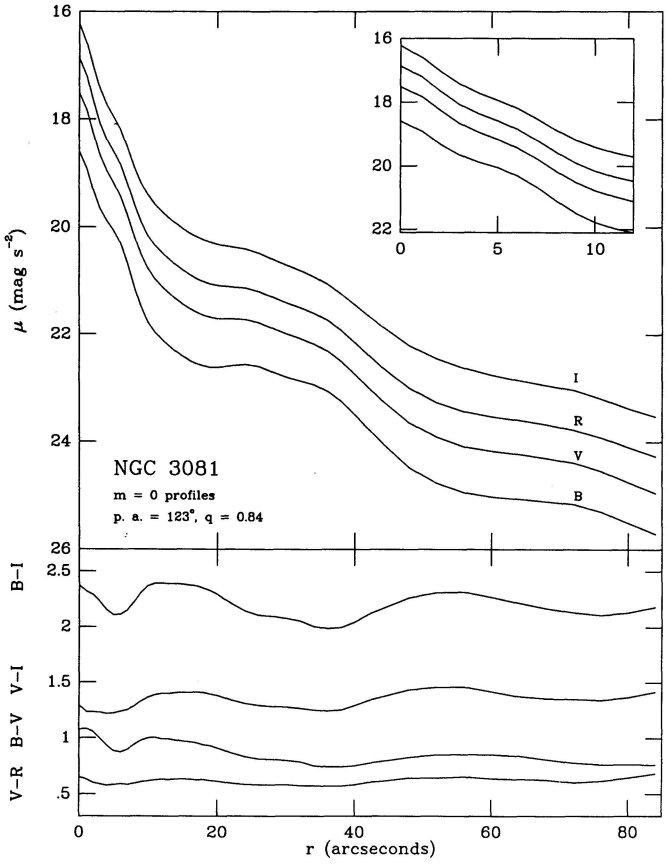

FIG. 12.—Azimuthally averaged surface brightness and color profiles of NGC 3081.

TABLE 5

AZIMUTHALLY AVERAGED PROFILES (mag s^{-2})

$r('')$	μ_V	$\mu_B-\mu_V$	$\mu_V-\mu_R$	$\mu_V-\mu_I$	$\mu_B-\mu_I$
0.0	17.51	1.08	0.65	1.29	2.37
1.1	17.84	1.08	0.63	1.23	2.32
2.1	18.27	1.05	0.60	1.23	2.29
3.0	18.66	0.99	0.59	1.23	2.23
4.0	18.94	0.93	0.58	1.22	2.15
5.0	19.17	0.89	0.58	1.22	2.11
6.0	19.43	0.87	0.59	1.24	2.11
7.0	19.77	0.90	0.58	1.25	2.15
8.0	20.16	0.94	0.59	1.29	2.23
9.0	20.51	0.98	0.61	1.33	2.31
10.0	20.77	1.00	0.62	1.37	2.37
11.0	20.96	1.00	0.62	1.39	2.39
12.0	21.11	0.99	0.63	1.40	2.39
13.0	21.23	0.99	0.63	1.40	2.39
14.0	21.34	0.98	0.63	1.41	2.39
15.0	21.43	0.97	0.63	1.41	2.38
16.0	21.52	0.97	0.63	1.41	2.38
17.0	21.59	0.96	0.62	1.41	2.37
18.0	21.64	0.94	0.63	1.41	2.35
19.0	21.68	0.93	0.62	1.39	2.33
20.0	21.70	0.91	0.61	1.38	2.29
21.0	21.71	0.89	0.60	1.36	2.25
22.0	21.71	0.87	0.60	1.34	2.21
24.0	21.72	0.83	0.59	1.31	2.14
26.0	21.78	0.81	0.58	1.29	2.11
28.0	21.89	0.81	0.58	1.29	2.10
30.0	21.99	0.80	0.58	1.28	2.08
32.0	22.08	0.79	0.57	1.27	2.05
34.0	22.18	0.75	0.57	1.25	2.00
36.0	22.31	0.74	0.57	1.25	1.99
38.0	22.50	0.74	0.57	1.25	2.00
40.0	22.73	0.75	0.58	1.29	2.05
42.0	22.99	0.78	0.60	1.34	2.11
44.0	23.23	0.79	0.61	1.37	2.16
48.0	23.64	0.83	0.64	1.43	2.26
52.0	23.91	0.85	0.64	1.46	2.31
56.0	24.09	0.85	0.65	1.46	2.31
60.0	24.17	0.85	0.64	1.42	2.27
64.0	24.22	0.84	0.63	1.37	2.21
68.0	24.30	0.81	0.62	1.36	2.17
72.0	24.38	0.78	0.60	1.35	2.13
76.0	24.53	0.77	0.62	1.34	2.11
80.0	24.74	0.76	0.64	1.37	2.13
84.0	24.94	0.76	0.68	1.42	2.18

Relative Fourier amplitudes in the B and I passbands (i.e., the total amplitude of the m-Fourier component with respect to the mean intensity at a given radius, I_0) are shown in the top panels of Figure 13. These allow us to estimate the relative apparent strength of the primary bar in NGC 3081 as compared to that in NGC 1433. The I band amplitudes are used since those in blue light are greatly affected by the star formation in the inner and nuclear rings. The amplitude profiles show a characteristic shape which is due mostly to the significant intrinsic elongation of the inner ring. Within the primary bar region the maximum relative amplitude of the 2θ Fourier term in NGC 3081 occurs at $r/r_{25} = 0.22$–0.25 at a value of $I_2/I_0 = 0.26$, or 45% of the same amplitude found for NGC 1433 (see dotted curve in the upper right-hand panel of Fig. 13). Thus we can say that the primary bar of NGC 3081 is slightly more than a factor of 2 weaker relative to the interbar regions than that in NGC 1433. However, the 2θ relative amplitude increases rapidly to $I_2/I_0 = 0.82$ at $r/r_{25} = 0.54$ compared to a peak of 0.95 found for NGC 1433. In spite of the apparently weaker primary bar, the inner ring of NGC 3081 produces a 2θ Fourier component comparable in amplitude to that in NGC 1433. However, this result depends on the choice of orientation parameters, and if the outer ring is an oval aligned perpendicular to the bar, then my analysis is overestimating the Fourier amplitudes due to the inner ring and underestimating those due to the outer ring.

The amplitudes of the three lowest odd Fourier terms are shown in the middle panels of Figure 13. In the I band, the odd terms are absolutely negligible across the entire zone occupied by the inner ring, and some small $m = 1$ amplitude becomes apparent only in the outer ring region. These highlight the extraordinary level of symmetry present in a galaxy like NGC 3081. Similar characteristics were found for NGC 1433.

The bottom panels of Figure 13 show the phases of the even Fourier components versus the radius. The phase of the I band 2θ term is uniform over the radius range $0.14 \leq r/r_{25} \leq 1.18$: well beyond the radius of the inner ring which extends to $r/r_{25} \sim 0.56$. Owing to the limited field of the CCD frame, the Fourier analysis could not be extended to the region beyond the outer ring.

f) *Ring Colors*

Finally, the colors of each ring were measured by integrating the surface photometry along the ridge lines in roughly equally spaced, small circular apertures. These positions are shown in the upper right panel of Figure 14. The individual color estimates for the inner ring are given in Table 6, while Table 7 summarizes the mean colors of all three rings. The ridge line colors are plotted versus apparent position angle on the sky in the other panels of Figure 14. Particularly interesting are the azimuthal color profiles for the inner ring. These show an obvious near-sinusoidal variation having an amplitude of 0.28 mag in $B-I$. The variation is in the sense that the ring is bluest along its major axis, which as already shown corresponds very closely with the bar axis as well. The trend for neither the outer ring nor the nuclear ring is so clear and well-defined. As shown in Figure 15, the inner ring is also brighter near its major axis than its minor axis, the total amplitude of the variation being about 0.50 mag s^{-2}.

In NGC 1433, the color variation around the inner ring is somewhat different from what is found here. In that object, the inner ring is reddest in those regions immediately trailing the bar rather than near its minor axis zone. The color variation is also more complex in other parts of the ring than is seen in NGC 3081.

V. DISCUSSION

The analysis above shows that NGC 3081 is similar in many ways to NGC 1433. The main differences seem to lie in the apparent strength of the primary bar, the azimuthal variation in colors around the inner ring, the faintness and morphological indistinctness of the outer ring, the earlier Hubble type, and the fact that NGC 3081 is a Seyfert while NGC 1433 is not. As for NGC 1433, many of the observed properties of the rings of NGC 3081 are consistent with the properties of rings which form near the main bar/orbit resonances in numerical simulations (to be discussed). These models allow the following determinations to be made.

a) *The Inner Ring*

The inner ring of NGC 3081 is probably linked with the inner 4:1 resonance where $\Omega_p = \Omega - \kappa/4$, Ω_p being the pattern speed of the bar, Ω the circular angular velocity, and κ the

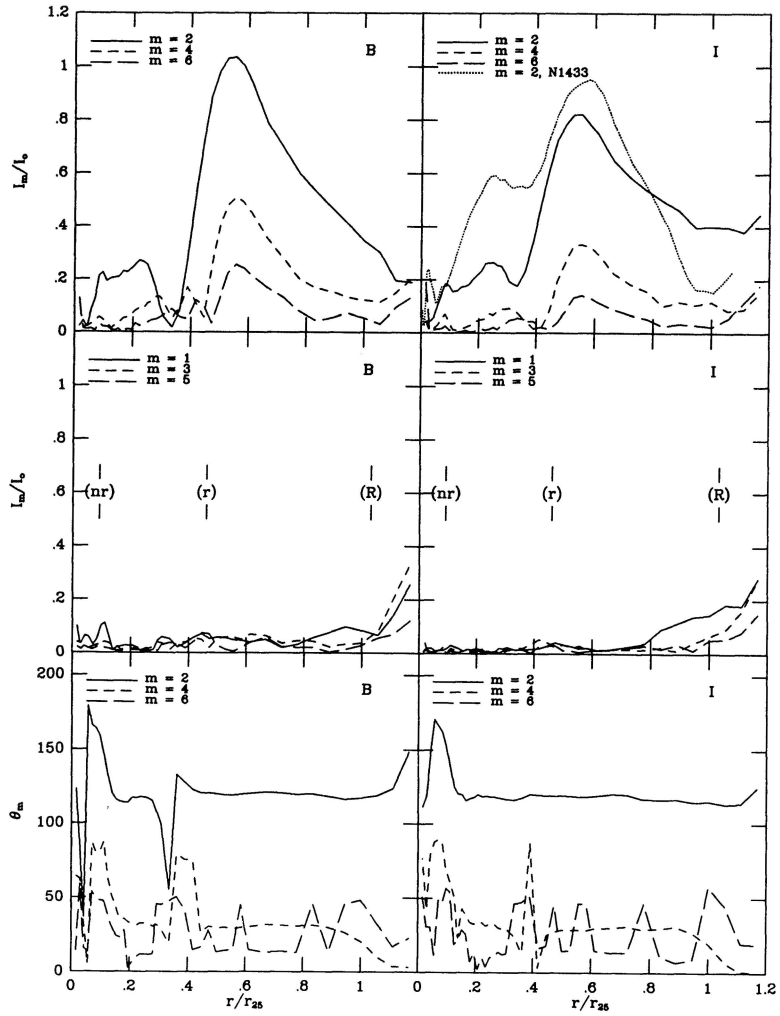

FIG. 13.—Relative Fourier intensity amplitudes (I_m/I_0) for series terms $m = 1$–6 and Fourier phases for $m = 2$, 4, and 6, plotted as a function of relative radius, r/r_{25}, where r_{25} is the radius of the $\mu_B = 25.0$ mag s^{-2} isophote. Positions of the inner, outer, and nuclear rings are shown. The upper right panel also shows for comparison the $m = 2$ relative amplitudes for NGC 1433.

epicyclic frequency. This particular resonance has been the subject of much recent analytical study (Contopoulos and Grosbol 1986; 1988; Contopoulos 1988), and in the case of barred galaxies was shown by Schwarz (1979, 1984*b*) to be capable of forming a gaseous ring elongated along the bar axis that would be located just inside corotation (CR). Schwarz (1984*b*) showed that the process works best only if the bar is strong enough to cause perturbed periodic orbits to cross at the resonance. If the bar is too weak, a ring is not likely to form there at all. The evolution of a 4:1 resonance ring, illustrated by Simkin, Su, and Schwarz (1980), is from a fairly open, four-armed spiral pattern, to a closed, slightly pointed oval of gas. A possible signature of incomplete evolution is breaks in the ring near the minor axis line of the bar. These breaks and the general character of the ring as a four-part structure are observed in the inner ring of NGC 1433.

The form, shape, orientation, and star formation properties of the inner ring of NGC 3081 are thus important to Schwarz's interpretation, and some details do agree with the theory. That gas dynamics are important to the ring is clear from the colors: the ring is a zone of currently active star formation, especially near its major axis. This is further supported by narrow-band Hα images by Durret and Bergeron (1986) and Pogge (1989), who showed that H II regions are also concentrated in arcs around the ring major axis. Another characteristic shown by the broad-band images is that the inner ring is not a perfect ellipse but is slightly pointed near its major axis. The ring has its greatest width in this region, and the pointiness would be expected only if the orbits come closest to CR there; it would also be expected if there were significant harmonics in the bar field (Schwarz 1984*b*). However, while the ring gives the impression that it is made of two tightly wound arms, within the seeing limitations there do not appear to be any breaks near its minor axis. This could imply that we are observing NGC 3081 in the most advanced phase of its ring evolution. The *n*-body model illustrated by Simkin, Su, and Schwarz (1980) shows an inner ring whose shape resembles that in NGC 3081.

The significant noncircular shape of the inner ring is one of the most interesting findings from this study. The ring has an intrinsic axis ratio comparable to or less than the average for SB galaxies. Schwarz (1984*b*, 1985) has discussed the factors affecting the intrinsic axis ratios of inner rings. One of the most important is bar strength, in the sense that if the bar is strong

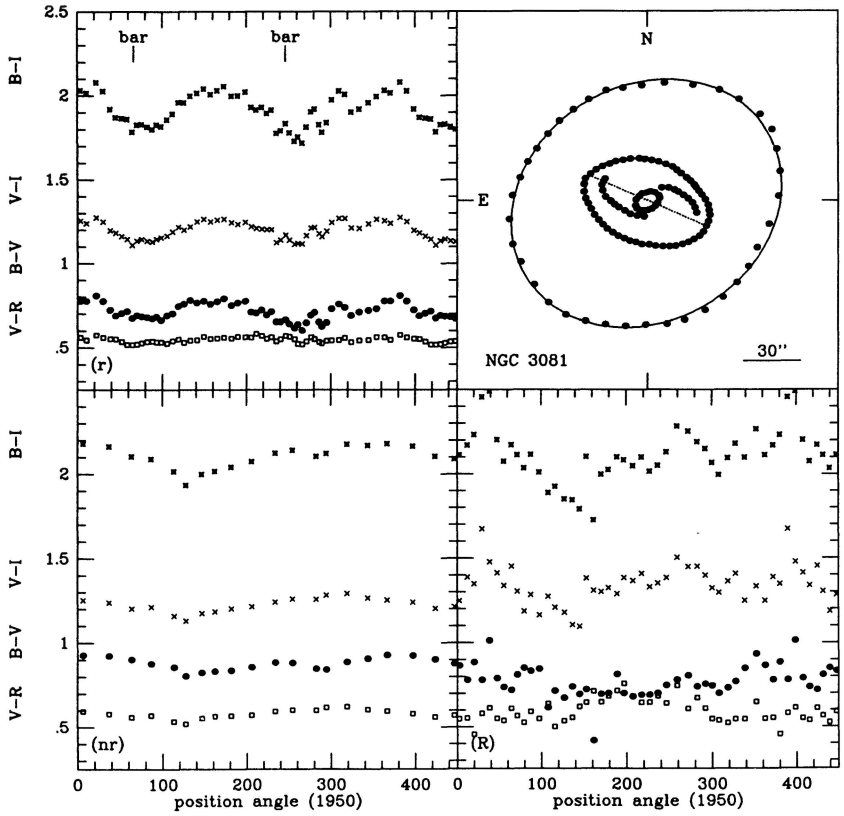

FIG. 14.—Azimuthal ridge-line color profiles of the rings of NGC 3081. The ridge-line positions used are shown in the schematic of the upper right-hand panel, which also shows the dust lanes and a line to indicate the position angle of the primary bar. Note the significant variation in the color around the inner ring.

enough to make orbits cross near the 4:1 resonance, then the ellipticity of the resulting ring will be greater for larger bar amplitudes. Together NGC 3081 and NGC 1433 suggest that rather different apparent bar strengths can produce rings of similar ellipticity. Since most real rings are not as oval as in these two and usually do not have sharp corners, Schwarz (1985) explored the effect of a lens structure underlying the ring. The presence of this structure tended to make the simulated rings rounder and less pointy. In the cases of both NGC 1433 and 3081, *I* band surface photometry reveals either a lens or an old stellar ring at the same position as the blue zone of star formation. In the presence of significant lenses, the inner rings are therefore still fairly elongated compared to the average.

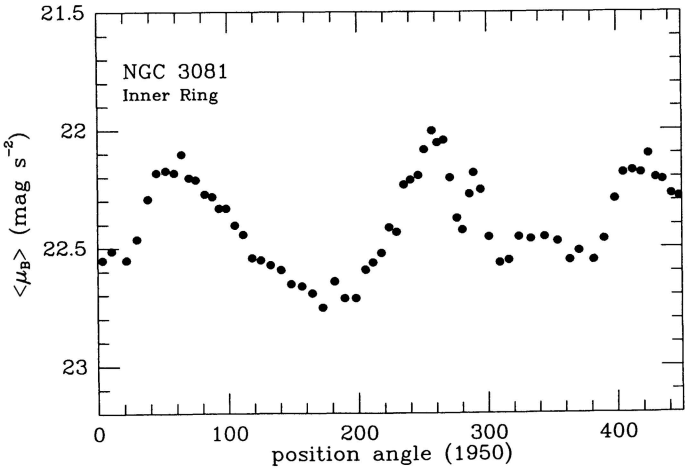

FIG. 15.—The variation in the average surface brightness within a 5″ aperture around the inner ring of NGC 3081. This shows that the ring achieves its highest surface brightness near its major axis at p.a. = 71° and 251°.

If the derived intrinsic shape of the inner ring of NGC 3081 is not seriously in error due to error in the inclination and line of nodes, then we can find a natural explanation for the significant azimuthal color variation. The orientation of the ring almost exactly along the bar axis suggests that it is wholly confined within CR. According to Contopoulos (1979), stars inside CR would stay longer at the apocentra of their orbits. If the gas is gathered into one of these orbits near CR, then we would expect more compression to occur in the major axis regions, and more active star formation. This could lead to a color variation that would resemble that seen in the inner ring of NGC 3081.

The more elongated than average shape of the inner ring of NGC 3081 suggests two interpretations: (1) that bar strength alone does not determine the ring shape; or (2) that NGC 3081 once had a stronger, more important bar than it has now. The idea of secular dissolution of bars was first proposed by Kormendy (1979) to explain the existence of lenses and has found some observational support (Kormendy 1984). However, *n*-body models (Miller and Smith 1979*a*, *b*; Combes and Sanders 1981; Carnevali 1983; Sparke and Sellwood 1987) have generally produced bars which are remarkably robust and persist for many bar rotations. There have been no simulations of how a bar might form quickly, generate an exception-

TABLE 6

RIDGE LINE COLORS OF THE INNER RING

Position Angle (1950)	r (″)	$<\mu_B>$ mag s^{-2}	$B-V$	$V-R$	$V-I$	$B-I$
3.67	22.09	22.55	0.78	0.56	1.25	2.03
10.75	22.82	22.51	0.77	0.54	1.24	2.01
21.89	23.93	22.55	0.81	0.57	1.27	2.08
30.11	25.03	22.46	0.78	0.56	1.25	2.03
38.35	26.52	22.29	0.72	0.55	1.20	1.92
44.96	27.72	22.18	0.69	0.55	1.18	1.87
52.04	29.48	22.17	0.70	0.53	1.16	1.87
58.49	31.25	22.18	0.71	0.52	1.15	1.86
64.30	32.78	22.10	0.67	0.52	1.11	1.79
69.89	34.26	22.20	0.69	0.52	1.14	1.83
75.25	34.14	22.21	0.68	0.53	1.15	1.83
82.01	33.42	22.27	0.68	0.53	1.14	1.82
87.85	32.15	22.28	0.67	0.54	1.13	1.80
93.00	30.93	22.33	0.68	0.53	1.15	1.83
98.61	29.73	22.33	0.66	0.53	1.16	1.82
105.36	28.67	22.40	0.69	0.53	1.17	1.86
111.77	27.31	22.44	0.70	0.54	1.19	1.89
118.75	26.33	22.54	0.74	0.55	1.22	1.96
125.59	25.58	22.55	0.76	0.53	1.20	1.96
133.06	24.62	22.57	0.78	0.54	1.22	2.00
140.98	24.11	22.59	0.77	0.54	1.25	2.01
148.87	23.41	22.65	0.77	0.56	1.27	2.04
157.10	23.17	22.66	0.76	0.55	1.25	2.01
164.95	22.81	22.69	0.77	0.55	1.26	2.03
172.98	23.20	22.75	0.79	0.56	1.27	2.06
181.91	23.42	22.64	0.75	0.56	1.25	2.00
189.73	24.45	22.71	0.76	0.56	1.24	2.00
198.35	25.47	22.71	0.78	0.56	1.25	2.02
205.64	26.90	22.59	0.71	0.56	1.22	1.93
211.58	28.17	22.56	0.71	0.58	1.21	1.92
218.10	29.40	22.52	0.72	0.57	1.21	1.93
224.09	30.56	22.41	0.69	0.55	1.20	1.90
229.73	31.64	22.43	0.71	0.56	1.20	1.91
235.40	32.84	22.23	0.65	0.54	1.13	1.78
240.47	33.50	22.21	0.65	0.55	1.14	1.79
246.41	33.56	22.19	0.66	0.57	1.17	1.84
250.99	33.68	22.08	0.64	0.57	1.14	1.78
256.89	33.30	22.00	0.62	0.55	1.11	1.73
261.00	32.36	22.05	0.64	0.52	1.12	1.76
265.91	31.58	22.04	0.60	0.52	1.12	1.72
271.10	30.01	22.20	0.65	0.54	1.17	1.81
276.27	28.41	22.37	0.69	0.56	1.21	1.91
280.60	27.19	22.42	0.71	0.55	1.21	1.92
285.95	26.23	22.27	0.65	0.53	1.18	1.83
289.28	25.65	22.18	0.62	0.52	1.16	1.78
294.81	24.71	22.25	0.65	0.54	1.19	1.84
301.05	23.81	22.45	0.73	0.54	1.25	1.98
309.51	22.81	22.56	0.76	0.54	1.27	2.03
316.49	22.22	22.55	0.74	0.56	1.27	2.01
324.19	22.23	22.45	0.69	0.53	1.21	1.90
333.45	21.62	22.46	0.71	0.54	1.21	1.92
344.30	21.46	22.45	0.72	0.55	1.24	1.96
354.13	21.47	22.47	0.73	0.56	1.26	1.99

ally oval inner ring, and then largely dissolve leaving the position, shape, and orientation of the ring intact.

b) *The Nuclear Ring*

The best interpretation of the nuclear ring is that it lies in the region of the inner Lindblad resonances. Most galaxies with a strong central peak and a low enough pattern speed are likely to have at least two ILRs, and orbit properties become very important near them (Contopoulos 1979). Dissipation in this region can lead to an oval or ring of gas whose major axis has an oblique angle with respect to the bar (Schwarz 1979; Combes and Gerin 1985). A wide range of true shapes seems possible from the models; however, statistics suggest that nuclear rings in general have nearly round intrinsic shapes.

TABLE 7

MEAN RING COLORS[a]

Feature	Aperture	$\langle B-V\rangle$ s.d.	$\langle V-R\rangle$ s.d.	$\langle V-I\rangle$ s.d.	$\langle B-I\rangle$ s.d.	n
(nr)	2″	0.87	0.58	1.22	2.09	16
		0.04	0.03	0.05	0.07	
(r)	5	0.71	0.55	1.20	1.91	53
		0.05	0.02	0.05	0.10	
(R)	10	0.76	0.60	1.33	2.09	38
		0.10	0.07	0.11	0.16	

[a] s.d. = standard deviation; n = number of ridge line positions.

That gasdynamics play a role in the nuclear ring of NGC 3081 is suggested from the color index map, since the ring is a zone of currently active star formation. However, it is interesting that Hα images do not show a ringlike form in this region. Instead, the images by Durret and Bergeron (1986) and Pogge (1989) show that Hα fills the entire nuclear oval zone. The same characteristic was found for the nuclear ring/lens in NGC 1433 (Buta 1986*b*), but not for the nuclear ring of NGC 1512 (Buta 1988).

From the ridge line of the color enhancement, the major axis position angle of the nuclear ring is 115°. If the dust lanes in the bar and the weak spiral arms emerging from the ring are curved in a trailing sense, then the major axis of the nuclear ring lies along an oblique angle with respect to the trailing side of the bar, about 131° in projection. This result does not depend significantly on the adopted orientation parameters since the galaxy is nearly face-on; hence, it supports the interpretation of the structure as being linked to the existence of an ILR in the inner parts of the bar.

Other galaxies with nuclear rings have been similarly interpreted, but the oblique phase with respect to the bar is not always seen. Also, the shapes are not always regular, especially in spirals of intermediate to late Hubble type. Particularly interesting examples in intermediate-type spirals recently studied in the context of the ILR interpretation are NGC 1068 (Telesco and Decher 1988) and NGC 4321 (Arsenault *et al.* 1988). In the former case the nuclear ring is really a pseudoring or tight inner spiral.

c) *The Bar and Dust Lanes*

The shape of the bar of NGC 3081 is certainly of interest but hard to quantify since it is weak. In blue light the bar actually appears to end short of the ring and looks somewhat boxy. On SRC J and ESO R Sky Survey charts, the bar also appears to underfill the inner ring. In the I band the bar shows a more elongated iosphote whose ends appear merged with the inner ring in Figure 5. The differences between B and I may be partly due to the dust lanes, which as in more prominent barred spirals, lie on the leading edges of the bar. The dust lanes are very subtle, but it seems clear that they are not very straight. Athanassoula (1988) has done numerical simulations to determine what factors control the straightness of such dust lanes. She found that in addition to the requirement that the x_2 family of orbits be present (ILR; Contopoulos 1979), the most curved dust lanes result when the axial ratio (b/a) of the bar is large (or alternatively, the bar is "fat"). The bar of NGC 3081 is not especially elongated (axis ratio ≈ 0.4), and the dust lane morphology seems consistent with Athanassoula's work.

An important question concerns the extent of the bar. Contopoulos (1980) favored that bars end at CR because the orbits beyond CR are aligned perpendicular to the bar and do not support it. However, Petrou and Papayannopoulos (1986) suggested that some bars might end near the 1:1 resonance owing to the stochastic effects introduced by a Feigenbaum sequence at that resonance. The 1:1 resonance does not always exist, but it seems to be favored for bars where the axis ratio $(b/a) < 0.2$. If this resonance does not exist, then Petrou and Papayannopoulos favored bars ending near the 3:1 resonance for a similar reason.

Although it is difficult to evaluate the results of Petrou and Papayannopoulos in the case of NGC 3081, it nevertheless appears that CR must lie somewhat beyond the ends of the optical bar of the galaxy. If the inner ring is linked with the 4:1 resonance, then the extent of the bar could be limited by one of the lower-order resonances. It is not likely to be the 1:1 resonance in this case because the nuclear ring favors the existence of ILR (2:1) well inside the bar. However, the more oval zone associated with the inner ring, which in the *I* band appears more like a lens, probably extends very close to CR. This feature, which is only mildly oval compared to the bar, probably contains a lot of mass and may constitute, on its own, a significant nonaxisymmetric disturbance.

d) The Outer Ring

The outer ring of NGC 3081 is one of the faintest and represents only a weak enhancement. It is likely that this feature is linked with the outer Lindblad resonance. A type identification for the feature (that is, R_1 or R_2) is difficult to make from morphology since there is little spiral character and no "dimpling" (see Buta 1986*a*) in the regions where the feature connects to the inner ring. However, the outer ring is brightest in those regions ($\mu_B = 24.7$ mag s^{-2}) as well as slightly bluer than at its major axis (where $\mu_B = 25.6$ mag s^{-2}). This suggests that it is an R_1 type and could be intrinsically elongated perpendicular to the bar since statistics imply this characteristic (Buta 1986*a*). If this is true, then my adopted orientation parameters are making the inner ring more elongated than it really is. More detailed kinematic studies could allow a better evaluation of this possibility. Also, H I studies would be essential to assess the gas content of the outer ring in particular and the galaxy as a whole. Such studies have recently been made for the ($R_1 R_2'$) galaxies NGC 1291 and NGC 5101 by van Driel, Rots, and van Woerden (1988), who found considerable concentrations of H I gas in the outer ring structures.

e) Resonance Identifications from Ring Ratios

Ring ratios have been studied by Athanassoula *et al.* (1982) and Buta (1984, 1986*a*). For a V = constant rotation curve, the expected size ratios of the principal resonances are $r(\mathrm{OLR})/r(\mathrm{CR}) = 1.7$, $r(\mathrm{OLR})/r(4{:}1) = 2.6$, and $r(\mathrm{OLR})/r(\mathrm{ILR}) = 5.8$. These ratios can be used to evaluate the ring identifications made above independently of the morphology and photometry (Athanassoula *et al.* 1982).

For NGC 3081, the projected outer-to-inner ring ratio, $d(\mathrm{R})/d(\mathrm{r}) = 2.22$, is in good agreement with similar estimates from larger samples made by Kormendy (1979), Athanassoula *et al.* (1982), and Buta (1986*a*). Since the inner ring has a significant intrinsic eccentricity, and the galaxy is inclined, a more appropriate estimate for comparison with the theoretical values is $d(\mathrm{R})/\langle d_0(\mathrm{r})\rangle = 2.40$, where $\langle d_0(\mathrm{r})\rangle$ is the face-on geometric mean diameter of the inner ring. If NGC 3081 has a flat rotation curve, then this ratio supports the interpretations made above, that the inner ring is linked with the inner 4:1 resonance and the outer ring with OLR.

The other interesting ratio, $d(\mathrm{r})/d(\mathrm{nr}) = 11.1$, is large compared to that expected if the outer ring is linked with OLR and the nuclear ring is linked with ILR, at least in the case of a flat rotation curve. In fact, for most galaxies with both rings, the ratio is usually larger than 10 (Buta 1984). This disagreement must reflect the fact that rotation curves in the vicinity of ILR are not usually flat but are steeply rising. In such circumstances even the relative position of ILR will depend on the rate of the rise to maximum velocity, which in turn depends on the central density and the amount of mass in the bulge. Thus, this ratio is less useful for unambiguous resonance identifications.

VI. CONCLUSIONS

NGC 3081 is a weakly barred, early-type disk galaxy with three clear ringlike enhancements: an exceptionally conspicuous inner ring of star formation, a nuclear ring of star formation, and a very faint outer ring. Morphological and photometric characteristics of this galaxy show that it has many features in common with NGC 1433, a prototype SB(r) type spiral with a strong bar. The properties of the three rings and dust lanes provide strong support for the interpretation of the rings in terms of the main orbit resonances expected in a barred galaxy.

There are, however, some contradictions to the theory which this object highlights well. There is a significant stellar component underlying the inner ring, yet that structure appears to be intrinsically more elongated than the average inner ring in SB or SAB galaxies. The extreme elongated shape is even more puzzling when we consider that the bar is much weaker in apparent strength than that in NGC 1433. Both NGC 1433 and NGC 3081 suggest that there is a poor correlation between apparent bar strength and intrinsic inner ring shape. However, of the four galaxies to be discussed in this series, the one with the most intrinsically circular inner ring, NGC 7187, also has the weakest evidence for a bar. This will be discussed further in Paper II (Buta 1990).

The structure of NGC 3081 may be providing a strong case for secular evolution in galaxy morphology. The inner ring is probably not a recently developed feature because it has a significant old component in addition to the young component (see Fig. 2). If a ring forms early when the bar is stronger, then even if the bar has been weakening it may be possible for the ring to survive intact. Even a weak bar may be able to maintain the star formation capabilities of the ring. However, if no significant secular evolution of the bar is occurring, then these results imply that bar strength or the existence of lenses are not the only factors affecting intrinsic ring shape. More numerical studies will be needed to assess the other factors which might be involved.

I would like to thank Dave Carter, Geoff Bicknell, and Shaun Hughes for obtaining the CCD observations of NGC 3081 for me while I was in a hospital recuperating from an accident incurred during my observing run. I would also like to thank Deborah Crocker and Agris Kalnajs for helpful comments on the manuscript and Deborah Crocker for her assistance in helping me to produce the many figures in this paper.

REFERENCES

Athanassoula, E. 1988, in *Proc. of the Joint Varenna-Abastumani International School and Workshop on Plasma Astrophysics* (ESA SP-285), Vol. **1**, p. 341.
Athanassoula, E., Bosma, A., Creze, M., and Schwarz, M. P. 1982, *Astr. Ap.*, **107**, 101.
Appenzeller, I., and Ostreicher, R. 1988, *A.J.*, **95**, 45.
Arsenault, R., Boulesteix, J., Georgelin, Y., and Roy, J.-R. 1988, *Astr. Ap.*, **200**, 39.
Bender, R., and Möllenhoff, C. 1987, *Astr. Ap.*, **177**, 71.
Boisson, C., and Durret, F. 1986, *Astr. Ap.*, **168**, 32.
Buta, R. 1984, Ph.D. thesis, University of Texas.
———. 1986*a*, *Ap. J. Suppl.*, **61**, 609.
———. 1986*b*, *Ap. J. Suppl.*, **61**, 631.
———. 1988, *Ap. J. Suppl.*, **66**, 233.
———. 1989, in *The World of Galaxies*, ed. H. Corwin, Jr. and L. Bottinelli (New York: Springer-Verlag), p. 29.
———. 1990, *Ap. J.*, submitted (Paper II).
Buta, R., and de Vaucouleurs, G. 1982, *Ap. J. Suppl.*, **48**, 219.
———. 1983*a*, *Ap. J. Suppl.*, **51**, 149.
———. 1983*b*, *Ap. J.*, **266**, 1.
Carnevali, P. 1983, *Ap. J.*, **265**, 701.
Combes, F., and Gerin, M. 1985, *Astr. Ap.*, **150**, 327.
Combes, F., and Sanders, R. H. 1981, *Astr. Ap.*, **96**, 164.
Contopoulos, G. 1979, in *Photometry, Kinematics, and Dynamics of Galaxies*, ed. D. S. Evans (Austin: University of Texas Press), p. 425.
———. 1980, *Astr. Ap.*, **81**, 198.
———. 1988, *Astr. Ap.*, **201**, 44.
Contopoulos, G., and Grosbol, P. 1986, *Astr. Ap.*, **155**, 11.
———. 1988, *Astr. Ap.*, **197**, 83.
de Vaucouleurs, G. 1948, *Ann. d'Ap.*, **11**, 47.
———. 1953, *M.N.R.A.S.*, **113**, 134.
———. 1977, in *The Evolution of Galaxies and Stellar Populations*, ed. B. Tinsley and R. Larson (New Haven: Yale University Observatory), p. 43.
de Vaucouleurs, G., and Buta, R. 1980*a*, *A.J.*, **85**, 637.
———. 1980*b*, *Ap. J. Suppl.*, **44**, 451.
de Vaucouleurs, G., and de Vaucouleurs, A. 1964, *Reference Catalogue of Bright Galaxies* (Austin: University of Texas Press).
de Vaucouleurs, G., de Vaucouleurs, A., and Corwin, H. G. 1976, *Second Reference Catalogue of Bright Galaxies* (Austin: University of Texas Press) (RC2).
de Vaucouleurs, G., de Vaucouleurs, A., Corwin, H., Buta, R., Paturel, G., and Fouque, P. 1989, *Third Reference Catalogue of Bright Galaxies* (New York: Springer-Verlag), in preparation (RC3).
de Vaucouleurs, G., and Peters, W. L. 1981, *Ap. J.*, **248**, 395.
de Vaucouleurs, G., Peters, W. L., Bottinelli, L., Gouguenheim, L., and Paturel, G. 1981, *Ap. J.*, **248**, 408.
Durret, F., and Bergeron, J. 1986, *Astr. Ap.*, **156**, 51.
Kormendy, J. 1979, *Ap. J.*, **227**, 714.
———. 1982, in *Morphology and Dynamics of Galaxies* (Geneva: Geneva Observatory), p. 115.
———. 1984, *Ap. J.*, **286**, 116.
Landolt, A. U. 1983, *A.J.*, **88**, 439.
Longo, G., and de Vaucouleurs, A. 1983, *A General Catalogue of Photoelectric Magnitudes and Colors in the U, B, V System of 3,578 Galaxies Brighter than the 16th V-Magnitude* (University of Texas Monograph in Astronomy: No. 3).
———. 1985, *Supplement to the General Catalogue of Photoelectric Magnitudes and Colors in the U, B, V system* (University of Texas Monograph in Astronomy: No. 3A).
Martin, P. G., Thompson, I. B., Maza, J., and Angel, J. R. P. 1983, *Ap. J.*, **266**, 470.
Miller, R. H., and Smith, B. F. 1979*a*, *Ap. J.*, **227**, 407.
———. 1979*b*, *Ap. J.*, **227**, 785.
Petrou, M., and Papayannopoulos, T. 1986, *M.N.R.A.S.*, **219**, 157.
Phillips, M. M., Charles, P. A., and Baldwin, J. A. 1983, *Ap. J.*, **266**, 485.
Pogge, R. W. 1989, *Ap. J.*, **345**, 730.
Sandage, A. 1961, *The Hubble Atlas of Galaxies* (Washington: Carnegie Institute of Washington) (Publication 618).
Sandage, A., and Tammann, G. 1981, *A Revised Shapley-Ames Catalogue of Bright Galaxies* (Washington Carnegie Institute of Washington) (Publication 635).
Schwarz, M. P. 1979, Ph.D. thesis, Australian National University.
———. 1984*a*, *Astr. Ap.*, **133**, 222.
———. 1984*b*, *Proc. Astr. Soc. Australia*, **5**, 464.
———. 1985, *Proc. Astr. Soc. Australia*, **6**, 202.
Simkin, S. M., Su, H. J., and Schwarz, M. P. 1980, *Ap. J.*, **237**, 404.
Sparke, L., and Sellwood, J. A. 1987, *M.N.R.A.S.*, **225**, 653.
Telesco, C. M., and Decher, R. 1988, *Ap. J.*, **334**, 573.
van Driel, W., Rots, A. H., and van Woerden, H. 1988, *Astr. Ap.*, **204**, 39.
Véron, M. P. 1981, *Astr. Ap.*, **100**, 12.
Wardle, M., and Knapp, G. R. 1986, *A.J.*, **91**, 23.
Whittle, M. 1985, *M.N.R.A.S.*, **216**, 817.
Wilson, A. S., and Meurs, E. J. A. 1982, *Astr. Ap. Suppl.*, **50**, 217.

Note added in proof.—Using data in Table 3, the neutral hydrogen flux from RC3, and RC2 procedures, the hydrogen index of NGC 3081 is H I $= m_{21}^0 - B_T^0 = 2.1 \pm 0.2$. This is smaller than the average for S0/a galaxies (G. de Vaucouleurs and R. Buta, *A.J.*, **88**, 939 [1983]) and suggests that NGC 3081 is richer in neutral hydrogen compared to other galaxies of this type.

RONALD J. BUTA: Department of Physics and Astronomy, University of Alabama, Box 870324, Tuscaloosa, AL 35487